2024 IEEE/RSJ International Conference on Intelligent Robots and Systems (IROS)
October 14-18, 2024. Abu Dhabi, UAE

Design and Control of a Three-Dimensional Electromagnetic Drive System for Micro-Robots

Yunrui Zhang, Yueyue Liu, Qigao Fan, *Senior Member, IEEE*

***Abstract*— Three-dimensional electromagnetic field drive technology, as a cutting-edge remote wireless control method, is extensively utilized in the biomedical diagnosis and treatment of micro-robots. This paper presents the design of a three-dimensional electromagnetic drive system for micro-robots, leveraging a gradient magnetic field to achieve comprehensive automatic control in three axes. Firstly, we refine the iron core's end structure to produce an uniform gradient magnetic field throughout the three-dimensional space. Following that, the parameters at the end of the iron core are fine-tuned to meet the specifications for magnetic field gradient, magnetic flux density, and effective workspace. Then a three-dimensional electromagnetic drive system with strong magnetic field gradient is established, achieving a remarkable maximum gradient of 1.70 T/m at the center of the workspace. Compared with other systems, the gradient is significantly enhanced. Subsequently, we carry out a three-dimensional drive experiment for a micro-robot, confirming the system's driving efficacy. To enable precise path following for micro-robots within a three-dimensional space, we have formulated a control strategy rooted in micro-robot dynamics. The controller stability is guaranteed through the Lyapunov theory. Ultimately, a three-dimensional path following experiment is executed on the developed electromagnetic drive system. The experiment confirms the capability of our designed system which can achieve the three-dimensional closed-loop motion for the micro-robot.**

***Index Terms*—** Micro-robot, three-dimensional electromagnetic drive system, closed-loop control.

I. INTRODUCTION

With the development of precision medicine, the need for micro-manipulation tools is increasing. In most cases, micro-manipulation tools need to be directly connected to an external drive to ensure reliable operation [1]. Micro-manipulation tools have attracted research attention in many fields, in the field of bioengineering, micro-manipulation robot systems are used to precisely manipulate small biological cells, such as gene transfer injection and fiber manipulation. Such tools are divided into five main types according to which they are used, including optical tweezers [2], chemical reactions [3], electrostatic fields, acoustic fields and magnetic fields [4]. It is noteworthy that magnetic field based actuation methods have a great advantage in manipulating tiny objects in biological tissues, due to the fact that magnetic fields are highly permeable in most biological tissues [5], which are insensitive to low-frequency magnetic fields. In addition, magnetic micro-robots are able to travel through complex environments of tiny dimensions [6], due to their small size and can be manipulated remotely and wirelessly, when driven by a magnetic field. Therefore magnetic field-driven micro-robots provide micro-manipulation tools suitable for biomedical applications such as drug delivery, vascular sparing and cellular micro-manipulation [7].

Generally, magnetic field driving methods for micro-robots can be divided into rotating magnetic fields and gradient magnetic fields [8]–[11]. Systems driven by rotating magnetic fields exert magnetic torque on the micro-robot. To transform this applied torque into a forward driving force, magnetic micro-robots are often crafted with unique designs, such as a spiral structure. However, such field can introduce complexity to the micro-robot's structural design, potentially diminishing its control precision [12]. In contrast, gradient magnetic fields employ field gradients to exert magnetic forces directly onto the micro-robot, offering the flexibility to drive magnetic micro-robots of any shape.

There are some objects that can generate gradient magnetic fields, such as permanent magnets, Helmholtz coils, and iron cores [13]. Usually, permanent [14] are incorporated into the end-effectors of a robot arm, and controlling the task involves adjusting these end-effectors. In [15], a three-dimensional electromagnetic drive system of micro-robot for biomedical or microfluidic applications is developed. Such system consists of eight permanent magnets that can generate a magnetic flux density of up to 30 mT and a magnetic field gradient of 0.83 T/m in any direction. However, this method tends to be more complex and often requires a larger operational space [16].

The Maxwell coil is a device used to generate a constant gradient magnetic field, based on the magnetic field transformation formula in Maxwell's equations, but usually the gradient, i.e. the driving force, is too small to effectively drive a micro-robot in complex environments or live bodies. In [17], a combined Helmholtz coils and Maxwell coils electromagnetic drive system is designed, which can obtain any magnetic forces in three-dimensional. Such system can produce the magnetic field density up to a maximum of 0.0399 T/m.

In this paper, we introduce a novel three-dimensional electromagnetic drive system for micro-robots, capable of producing strong magnetic field gradients within a considerably fairly working area. Firstly, the shape of the core end is designed and the parameters of the core end are fine-tuned to

This work was supported in part by the National Natural Science Foundation of China under Grant 62373168, 62203186, and in part by the 2022 open research project of Guangxi Key Laboratory of Automobile Components and Vehicle Technology under Grant 2022GKLACVTKF06. (*Corresponding author: Yueyue Liu and Qigao Fan.*)

The authors are with the School of Internet of Things Engineering, Institute of Automation, Jiangnan University, Wuxi, 214122, China. E-mail: 1196140083@qq.com, yueyueliu@jiangnan.edu.cn, qgfan@jiangnan.edu.cn.

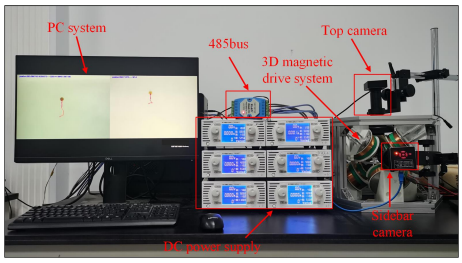

Fig. 1. Three-dimensional electromagnetic drive system experimental platform

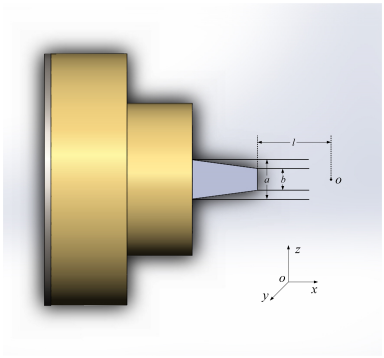

Fig. 2. Schematic diagram of the structural parameters of the iron core coil

achieve the required magnetic field gradient. Then, in order to achieve the three-dimensional motion control of the micro-robot, a gravity compensation method for the micro-robot is proposed and the effectiveness of the gravity compensation is experimentally demonstrated. Finally, a three-dimensional path following control method is proposed for the micro-robot. By conducting simulations and experiments, we can obtain that the micro-robot is capable of following various three-dimensional paths with impressive following precision.

II. MODELLING OF THREE-DIMENSIONAL ELECTROMAGNETIC DRIVE SYSTEM

The developed electromagnetic manipulation system comprises three pairs of iron coils arranged orthogonally. We choose the coils current driver as RD-S1005. The safety of coil power-on and appropriate magnetic field gradient are the primary factors in selecting a power supply, so a 5 A DC power is adopted in the system. The DC source can support RS232, CAN bus and RS485 multi-station communication. The output position of the micro-robot is measured in real-time by two CCD cameras with a frame rate of 60FPS and high sensitivity. The motion control algorithms are developed in real-time using the Python language on a host PC. The overall structure of the three-dimensional electromagnetic drive system is shown in Fig. 1.

A. Design the Workspace

Define the centre of the workspace, the bottom edge length of the core end, the top edge length and the distance from the core end to the centre of the workspace as O, a, b and l, respectively. the design of a, b and l can affect the magnetic field gradient, flux density and the uniformity significantly. Therefore, the parameters l, a and b are selected as our design variables for optimization. A schematic diagram of the core coil structure parameters is shown in Fig. 2.

In order to design the parameter l, we fixed the parameter as shown in Table I. We choose several representative parameters, i.e., 15, 20, 25, 30 and 35 mm, to analysis the relationship of l and flux density. The variation of flux density at different l is shown in Fig. 3. As can be seen from the graph, the flux density becomes progressively smaller as l increases, and too small l will result in a smaller workspace so that two cameras can't placed to obtain the 3D position of the micro-robot space. Based on above analysis, in this paper we choose $l = 25mm$ as the distance from the core end to the workspace centre.

TABLE I
PARAMETERS WHEN TUNING THE DISTANCE L FROM THE END OF THE IRON CORE TO THE CENTRE OF THE WORKSPACE

Iron core coil parameters	Values	Unit
First stage core radius	35	*mm*
Second stage iron core radius	25	*mm*
First stage core height	35	*mm*
second stage core height	30	*mm*
Length of the bottom edge of the iron core end	18	*mm*
Top edge length of core end	10	*mm*
Outer radius of the first stage coil	55	*mm*
Outer radius of second stage coil	32	*mm*
Number of turns of the first stage coil	600	circle
Number of turns in the second stage coil	200	circle
Current size	5	*A*

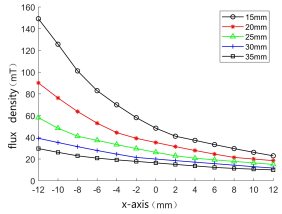

Fig. 3. Flux density variation curve at different l

B. Design the top and Bottom Edge Lengths

In this subsection we will design a and b to obtain the maximum magnetic field gradient. By keeping l constant and varying the bottom edge length a from 15 to 20 mm and the top edge length b from 6 to 10 mm, we can derive the flux density and magnetic field gradient at the center of the workspace for different values. This allows us to identify the structural parameters of the core end that yield the maximum magnetic field gradient. According to the Fig. 4, the magnetic field gradient is greatest at a value of 1.70 T/m for a = 18 mm and b = 10 mm, which produces 26.19 mT, We choose them as our top and bottom edge lengths.

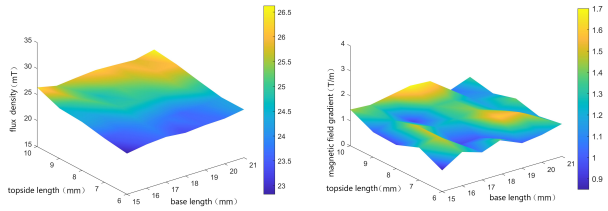

(a) Flux density (b) Gradient

Fig. 4. Different values of a and b.

C. Design the Overall Three-Dimensional Electromagnetic Drive system

By fine-tuning the structural parameters of the system, we determine the parameters for the individual core coils within the three-dimensional electromagnetic drive system designed for the micro-robot. Given the necessity for three-dimensional motion control of the micro-robot, compared with produce magnetic forces in the x-axis, y-axis, and z-axis directions, ensuring effective micro-robot motion.

Then, we design six identical core coils, arranged in pairs orthogonally and inclined within the outer structure, to create a 50 x 50 x 50 mm^3 workspace. The comprehensive structure of the three-dimensional electromagnetic drive system is illustrated in Fig. 5.

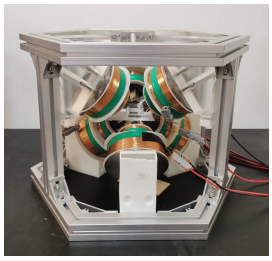

Fig. 5. Three-dimensional electromagnetic drive system

III. ANALYSIS OF MAGNETIC FIELD

A. Modelling of Finite Element

To model the generation of the magnetic field, we establish a finite element analysis framework. The 3D electromagnetic drive system, constructed in SolidWorks, is then imported into ANSYS Maxwell3D for a comprehensive finite element simulation.

In the simulation, the parameters are set according to the actual parameters of the core coil. The core is made of DT4E material, while the coil is designated as a stranded type, and the maximum incoming current is set according to the actual DC power supply, not exceeding 5 A. Based on the structure of the core coil, we establish a three-dimensional coordinate system for the entire magnetic field. As depicted in Fig. 6, using coil 1 as a reference, we define a three-dimensional local coordinate system $O-x_1y_1z_1$, where x_1, y_1, z_1 represents the axial direction of coil 1. Accordingly, for all coils, the local coordinate system can be similarly defined as $O-x_ky_kz_k$, with k ranging from 1 to 6. The origin for all these coordinate systems is situated at the center of the workspace and is represented by O.

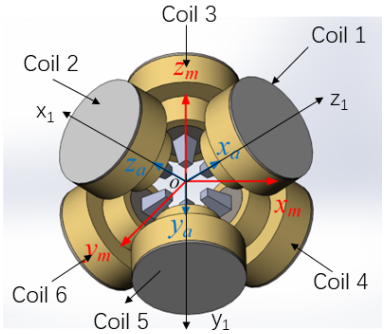

Fig. 6. System of coil

B. Consistent and Uniformity of Magnetic Field

To confirm that six individual core coils can generate consistent magnetic fields when supplied with the same current, we employ a Gaussian magnetometer probe. This probe measure the magnetic flux density at five points along the z_k axis (with k = 1, 2, 3, 4, 5, and 6), specifically at z_k positions of -10 mm, -5 mm, 0 mm, 5 mm, and 10 mm. Each of these individual core coils is powered with a 1 A current during these measurements.

Fig. 7 presents the measurement results. it's evident that the measurements for each of the six core coils at every position are fundamentally similar. While minor discrepancies exist, they are negligible, suggesting a consistent magnetic field generation across all six coils. Given this consistency, our analysis becomes more efficient: by examining just one core coil, we can extrapolate the collective behavior by layering the outcomes of individual coils.

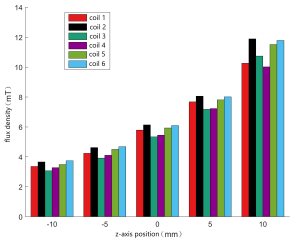

Fig. 7. Magnetic field measurement results for six core coils

C. Verification of Magnetic Field

The finite element model is validated, by comparing the finite element simulation results with the experimental measurements. Table II presents both the experimental and simulated outcomes for the magnetic flux density at z = -15, -5, and 5 mm for coil 1, with incoming currents set at 1, 2, and 3 A, respectively. As can be seen from Table II, it's evident that the discrepancy between the simulated and experimental flux density results, reaches a maximum error of 9.15% and a minimum of 4.02%, across distinct positions

and current inputs. While there are some discrepancies due to structural errors, current fluctuations, and unavoidable external environmental disturbances in the 3D electromagnetic drive system, the overall results still achieve a commendable level of accuracy and are quite satisfactory.

TABLE II
ERROR OF EXPERIMENTAL MEASUREMENT

Placement (*mm*)	Current (A)	Simulation (*mT*)	Experimental (*mT*)	Error (%)
z=5	1	15.34	16.02	4.24
	2	30.69	32.17	4.60
	3	46.03	49.01	6.08
z=-5	1	7.08	7.68	7.81
	2	14.17	15.09	6.09
	3	21.25	22.14	4.02
z=-15	1	4.02	4.24	5.19
	2	8.04	8.85	9.15
	3	12.06	13.18	8.50

D. Verification of Linear Relationship

Based on the Biot-Savart law [2], a linear relationship exists between the magnetic flux density and the current's magnitude. With the incorporation of the DT4E core in our electromagnetic drive system design, it became crucial to ascertain if this linear relationship is still evident. We conduct experimental measurements of the magnetic flux density at positions z = 0, 5, 10, and 15 *mm* for incoming currents ranging from 1 to 5 A. The results, presented in Fig. 8, clearly indicate that the magnetic flux density remains fundamentally linear with the incoming current.

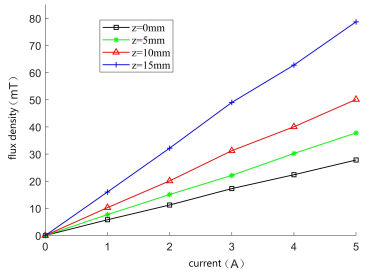

Fig. 8. The results of flux density and current measurement

IV. CONTROL OF CLOSED-LOOP MOTION

A. Micro-robot Dynamics Modelling

In three-dimensional space, the motion of the micro-robot is influenced by factors such as gravity, buoyancy, and fluid resistance, along with the magnetic force [18]. By comprehensively analyzing these forces, we derive the micro-robot's dynamics. The whole system is perturbed by the magnetic field noise, the liquid micro-flow caused by environmental vibration and other factors, which will be added to the micro-robot dynamics equation as an unknown term $\Delta = \begin{bmatrix}\Delta_x & \Delta_y & \Delta_z\end{bmatrix}^T$. Therefore the dynamics model of the micro-robot in the three-dimensional space is:

$$m\frac{d^2p}{dt^2} = F_{mag} + F_{drag} + F_b + G + \Delta \tag{1}$$

where F_b denotes the buoyancy of the micro-robot in the solution, G is the gravitational force of the micro-robot itself, and m is the mass of the micro-robot.

B. Three-dimensional Coordinate Rotation Transformation

Path following for robots in three-dimensional space is challenging as is shown in Fig. 9. Managing errors in both the *xoy* and *xoz* planes, while accounting for various external factors, adds to the complexity of the task.

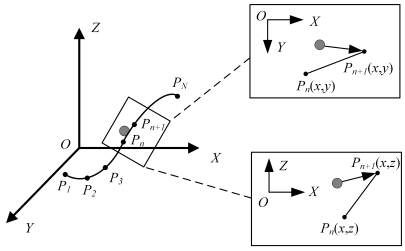

Fig. 9. Analysis of 3D path following

C. Path Following Controlling Design

Define the error variables E_1 and E_2 as:

$$\begin{cases} E_1 = e = p - p_r \\ E_2 = \dot{e} = \dot{p} - \dot{p}_r \end{cases} \tag{2}$$

where E_1 denotes the position error and E_2 denotes the velocity error. Combining with (2), then (1) can be transformed as:

$$\begin{cases} \dot{E}_1 = E_2 \\ \dot{E}_2 = b\mu + aE_2 + c + b\Delta \end{cases} \tag{3}$$

where $a = -6\pi\eta R/m$, $b = 1/m$, $c = -6\pi\eta R\dot{p}_r/m - \ddot{p}_r$ and $\mu = F_{mag}$ as an input to the system.

Then we will design a micro-robot 3D path following controller based on input-state stability theory and backstepping control to drive the micro-robot along the referenced path.

Based on (3), the controller can be designed as:

$$\mu = -\frac{1}{b}\left((1-K_1)E_1 + aE_2 + \left(\Gamma + K_1\frac{1}{2}\right)\tilde{E}_2 + c\right) \tag{4}$$

$\Gamma, K_1 > 0, \tilde{E}_2 = E_2 - E_2^*$ with $E_2^* = -\Gamma E_1$.

After determining the magnetic force μ, the magnitude of the current through the coil can be calculated by the pseudo-inverse technique [19], and then output through the DC power supply.

Theorem 1: Considering the system (3), the controller (4) guarantees that E_1 and $\tilde{E}_2$ inputs are stabilised with respect to the environmental uncertainties and disturbances, i.e., the position error and the velocity error are eventually bounded. In addition, the tracking error converges to zero if there are no uncertain disturbances.

Proof: Define a Lyapunov function

$$V_1 = \frac{1}{2}E_1^T E_1 + \frac{1}{2}\tilde{E}_2^T \tilde{E}_2 \tag{5}$$

Take the derivative of V_1 with respect to time t

$$\dot{V}_1 = -E_1^T \Gamma E_1 + \tilde{E}_2^T \left(E_1 + b\mu + aE_2 + c + b\Delta + \Gamma E_2\right) \quad (6)$$

Let

$$E_1 + b\mu + aE_2 + c + b\Delta + \Gamma E_2 = -K_1 \tilde{E}_2 \quad (7)$$

We can obtain

$$\begin{aligned} \dot{V}_1 &= -K_1 E_1^T E_1 + \tilde{E}_2^T \left(b\Delta - K_1 \tilde{E}_2\right) \\ &= -\tilde{E}_2^T K_1 \tilde{E}_2 + bS^T \Delta - E_1^T \Gamma E_1 \end{aligned} \quad (8)$$

According to the Youngs inequality, we can obtain

$$\tilde{E}_2^T \Delta \leqslant \frac{1}{2} \tilde{E}_2^T \tilde{E}_2 + \frac{1}{2} \Delta^T \Delta \quad (9)$$

From (9) and (8), we can obtain

$$\dot{V}_1 \leq -\tilde{E}_2^T \left(K_1 - \frac{b}{2}\right) \tilde{E}_2 + \frac{b}{2} \Delta^T \Delta - E_1^T \Gamma E_1 \quad (10)$$

let

$$\kappa = \min\left(\lambda_{min}\left(K_1 - \frac{b}{2} I\right), \lambda_{min}(\Gamma)\right), \varepsilon = \frac{b}{2} \Delta^T \Delta \quad (11)$$

$\lambda_{min}(\cdot)$ represents the minimum eigenvalue of $(\cdot)$. Finally, the equation turns to

$$\dot{V}_1 \leq -\kappa V_1 + \varepsilon \quad (12)$$

If there is no disturbance i.e.,$\Delta = 0$ and $\varepsilon = 0$, then the tracking error will converge to zero. The above equation is obtained by multiplying both sides of the equation by $e^{\kappa t}$ and also integrating over the interval [0, t]:

$$\begin{aligned} V_1 &\leq V_1(0) + \frac{\varepsilon}{k} - \frac{\varepsilon}{k} e^{-\kappa t} \\ &\leq V_1(0) + \frac{\varepsilon}{\kappa} \end{aligned} \quad (13)$$

Substituting (5) into (13) we can conclude that E_1 and $\tilde{E}_2$ are semiglobally uniformly ultimately bounded (SGUUB) and furthermore converge to the sets Ω_{E_1} and $\Omega_{\tilde{E}_2}$, defined as:

$$\Omega_{E_1} = \left\{ \|E_1\| \leq \sqrt{2\left(V_1(0) + \frac{\varepsilon}{\kappa}\right)} \right\} \quad (14)$$

$$\Omega_{\tilde{E}_2} = \left\{ \|\tilde{E}_2\| \leq \sqrt{2\left(V_1(0) + \frac{\varepsilon}{\kappa}\right)} \right\} \quad (15)$$

According to the dynamics equations of the micro-robot, we can obtain the position tracking error e and its derivative $\dot{e}$ are globally bounded. For the system perturbation Δ, the appropriate parameters Γ, K_1 can be chosen to suppress Δ. This ensures that the position tracking error of the micro-robot converges to a neighbourhood of the origin that is sufficiently small. ■

After Designing the controller, we take the experimental platform, which is shown in Fig. 1 to drive the micro-robot in three-dimensional space. The micro-robot used in the experiment has a diameter of 250 μm and a density of 1.8 g/cm^3, and the coefficient of viscosity of the liquid is $\eta = 0.2 mPa \cdot s$. Experimental container is located at the three-dimensional centre of the electromagnetic drive system. The controller parameters is same as the simulation.

We set the path of the micro-robot in three-dimensional space to be "N", and the micro-robot is driven by a given coil current to make its path "N". The process is divided into three stages, as shown in Fig. 10. The table III shows the three stages.

TABLE III
PARAMETERS OF THE TRAJECTORY STAGES

Stage	Time(s)	Energised coil	Current(A)
ab	0-2.2	Coil 13	2.2,2.2
bc	2.2-5.4	Coil 4,5,6	1.3,1.3,1.3
cd	5.4-7.4	Coil 1,3	2.5,2.5

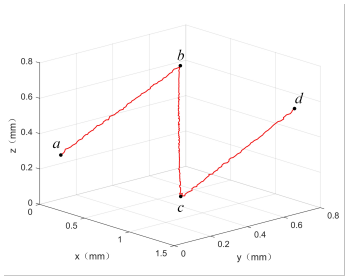

Fig. 10. Three-dimensional drive for micro-robot

According to the experimental results, the designed three-dimensional electromagnetic drive system is able to realise the micro-robot's motion path in three-dimensional space as "N", and it also proves the effectiveness of the three-dimensional electromagnetic drive system to drive the micro-robot.

V. EXPERIMENT

To further verify the effectiveness of the closed-loop control method by the proposed controller (4). Two experiments of three-dimensional tracking are conducted. It is worth noting that in our micro-robot tracking experiment, visual feedback employs traditional image thresholding, but advanced visual learning algorithms like deep learning could significantly boost performance, capturing nuanced target changes more precisely [20]–[23]. Consequently, exploring the application potential of these advanced visual learning technologies in the realm of micro-robots holds significant importance for further enhancing system performance and intelligence levels.

In the first experiment, the reference path is set as a 3D straight line. Fig. 11 shows the error of the micro-robot tracking the 3D straight line path and the path following results. In the second experiment, the reference path is set as a triangular path in 3D space. Fig. 12 shows the tracking error of the micro-robot tracking the triangular path and triangular path results.

From Fig. 11 and Fig. 12, we can obtain that both of the actual trajectories appear to coincide with the 3D reference paths in two experiments. In addition the minimum

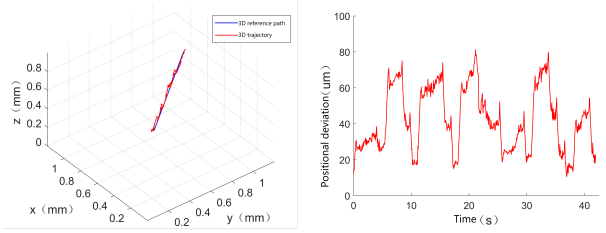

(a) Experimental results (b) tracking error

Fig. 11. Three-dimensional straight lines.

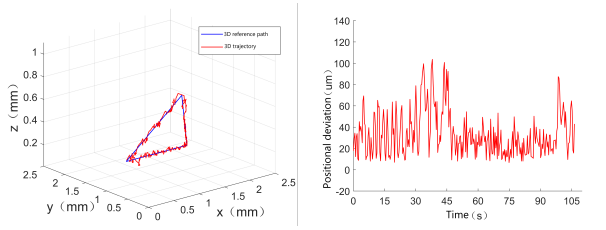

(a) Experimental results (b) tracking error

Fig. 12. Three-dimensional triangular path.

tracking errors only $8.14\mu m$ and $6.67\mu m$, which means a high tracking accuracy. While the maximum errors of trajectory no more than $81.13\mu m$ and $100.87\mu m$ because the inevitable disturbance. In addition, we can find the errors reach into an extremely small range and low average of error. Generally, the tracking errors are both bounded and reasonable. Therefore, the proposed control method can achieve the 3D path following with good tracking accuracy paths.

VI. CONCLUSIONS

In this paper, we design a three-dimensional electromagnetic drive system for micro-robot, which realises three-dimensional motion control of micro-robot by generating a gradient magnetic field. Firstly, designing the core end structure and choosing the parameters of the core end to meet the requirements of magnetic field gradient, magnetic flux density and workspace. The designed system can generate stronger magnetic field gradient than other systems. In addition, we design a three-dimensional closed-loop control of the micro-robot. Subsequently, the closed-loop stable system is guaranteed based on Lyapunov theory. Finally, both simulations and experiments prove that the method can verifies that the three-dimensional closed-loop control can achieve the micro-robot tracking of different kinds of paths.

REFERENCES

[1] G. Hwang, I. A. Ivan, J. Agnus, H. Salmon, S. Alvo, N. Chaillet, S. Rgnier, and A. M. Haghiri-Gosnet, "Mobile microrobotic manipulator in microfluidics," *Sensors & Actuators A Physical*, vol. 215, pp. 56–64, 2014.

[2] X. Li, H. Yang, J. Wang, and D. Sun, "Design of a robust unified controller for cell manipulation with a robot-aided optical tweezers system," *Automatica*, vol. 55, pp. 279–286, 2015.

[3] S. T. Chang, V. N. Paunov, D. N. Petsev, and O. D. Velev, "Remotely powered self-propelling particles and micropumps based on miniature diodes," *Nature Materials*, vol. 6, no. 3, pp. 235–40, 2007.

[4] K. E. Peyer, E. Siringil, L. Zhang, and B. J. Nelson, "Magnetic polymer composite artificial bacterial flagella," *Bioinspiration & Biomimetics*, vol. 9, no. 4, p. 046014, 2014.

[5] Z. Song, W. Zhang, W. Zhang, and D. Paolo, "A novel biopsy capsule robot based on high-speed cutting tissue," *Cyborg and Bionic Systems*, vol. 2022, 2022.

[6] W. Cheng, G. Yan, P. Gao, and Z. Wang, "Design and implementation of control system for colon diagnosis and treatment microrobot," *Optics and Precision Engineering*, vol. 20, no. 006, pp. 1296–1302, 2012.

[7] "Fabrication and characterization of magnetic microrobots for three-dimensional cell culture and targeted transportation," *Advanced Materials*, vol. 25, no. 41, pp. 5829–5829, 2013.

[8] J. Tian, B. Huang, M. H. Nawaz, and W. Zhang, "Recent advances of multi-dimensional porphyrin-based functional materials in photodynamic therapy," *Coordination Chemistry Reviews*, vol. 420, no. 6056, p. 213410, 2020.

[9] Y. Liu, H. Wang, and Q. Fan, "Adaptive learning and sliding mode control for a magnetic microrobot precision tracking with uncertainties," *IEEE Robotics and Automation Letters*, vol. 8, no. 11, pp. 7767–7774, 2023.

[10] H. Wang, Y. Liu, Q. Fan, X. Wu, and Y. Hu, "Adaptive neural network tracking for a magnetic microrobot in presence of model uncertainty and unknown disturbance," in *2023 IEEE 19th International Conference on Automation Science and Engineering (CASE)*. IEEE, 2023, pp. 1–6.

[11] Q. Fan, H. Wang, X. Wu, and Y. Liu, "Magnetic microrobot control based on a designed nonlinear disturbance observer," in *2023 International Conference on Advanced Robotics and Mechatronics (ICARM)*. IEEE, 2023, pp. 606–611.

[12] T. Y. Huang, M. S. Sakar, A. Mao, A. J. Petruska, F. Qiu, X. B. Chen, S. Kennedy, D. Mooney, and B. J. Nelson, "3d printed microtransporters: Compound micromachines for spatiotemporally controlled delivery of therapeutic agents," *Advanced Materials*, vol. 27, no. 42, pp. 6644–6650, 2016.

[13] D. Li, F. Niu, J. Li, X. Li, and D. Sun, "Gradient-enhanced electromagnetic actuation system with a new core shape design for microrobot manipulation," *IEEE Transactions on Industrial Electronics*, vol. 67, no. 6, pp. 4700–4710, 2020.

[14] P. Ryan and E. Diller, "Magnetic actuation for full dexterity microrobotic control using rotating permanent magnets," *IEEE Transactions on Robotics*, vol. 33, no. 6, pp. 1398–1409, 2017.

[15] C. Heunis, J. Sikorski, and S. Misra, "Flexible instruments for endovascular interventions: Improved magnetic steering, actuation, and image-guided surgical instruments," *IEEE Robotics & Automation Magazine*, vol. 25, no. 3, pp. 71–82, 2018.

[16] F. Niu, J. Li, W. Ma, J. Yang, and D. Sun, "Development of an enhanced electromagnetic actuation system with enlarged workspace," *IEEE/ASME Transactions on Mechatronics*, vol. 22, no. 5, pp. 2265–2276, 2017.

[17] Q. Zhang, S. Song, P. He, H. Li, H.-Y. Mi, W. Wei, Z. Li, X. Xiong, and Y. Li, "Motion control of magnetic microrobot using uniform magnetic field," *IEEE Access*, vol. 8, pp. 71 083–71 092, 2020.

[18] J. Lu, Y. Liu, W. Huang, K. Bi, Y. Zhu, and Q. Fan, "Robust control strategy of gradient magnetic drive for microrobots based on extended state observer," *Cyborg and Bionic Systems*, vol. 2022, 2022.

[19] X. Zhang, R. Jing, Z. Li, Z. Li, X. Chen, and C.-Y. Su, "Adaptive pseudo inverse control for a class of nonlinear asymmetric and saturated nonlinear hysteretic systems," *IEEE/CAA Journal of Automatica Sinica*, vol. 8, no. 4, pp. 916–928, 2021.

[20] Q. Fan, Y. Wu, K. Bi, and Y. Liu, "Autonomous vision-guided two-arm collaborative microassembly using learned manipulation model," *IEEE Robotics and Automation Letters*, vol. 9, no. 3, pp. 2375–2382, 2024.

[21] L. Yu, D. Liu, H. Mansour, and P. T. Boufounos, "Fast and high-quality blind multi-spectral image pansharpening," *IEEE Transactions on Geoscience and Remote Sensing*, vol. 60, pp. 1–17, 2021.

[22] Z. Kou, G. Cui, S. Wang, W. Zhao, and C. Xu, "Improve cam with auto-adapted segmentation and co-supervised augmentation," in *Proceedings of the IEEE/CVF Winter Conference on Applications of Computer Vision*, 2021, pp. 3598–3606.

[23] Z. Xie, S. Wang, W. Zhao, and Z. Guo, "Context attention module for human hand detection," in *2019 IEEE International Conference on Multimedia & Expo Workshops (ICMEW)*. IEEE, 2019, pp. 555–560.